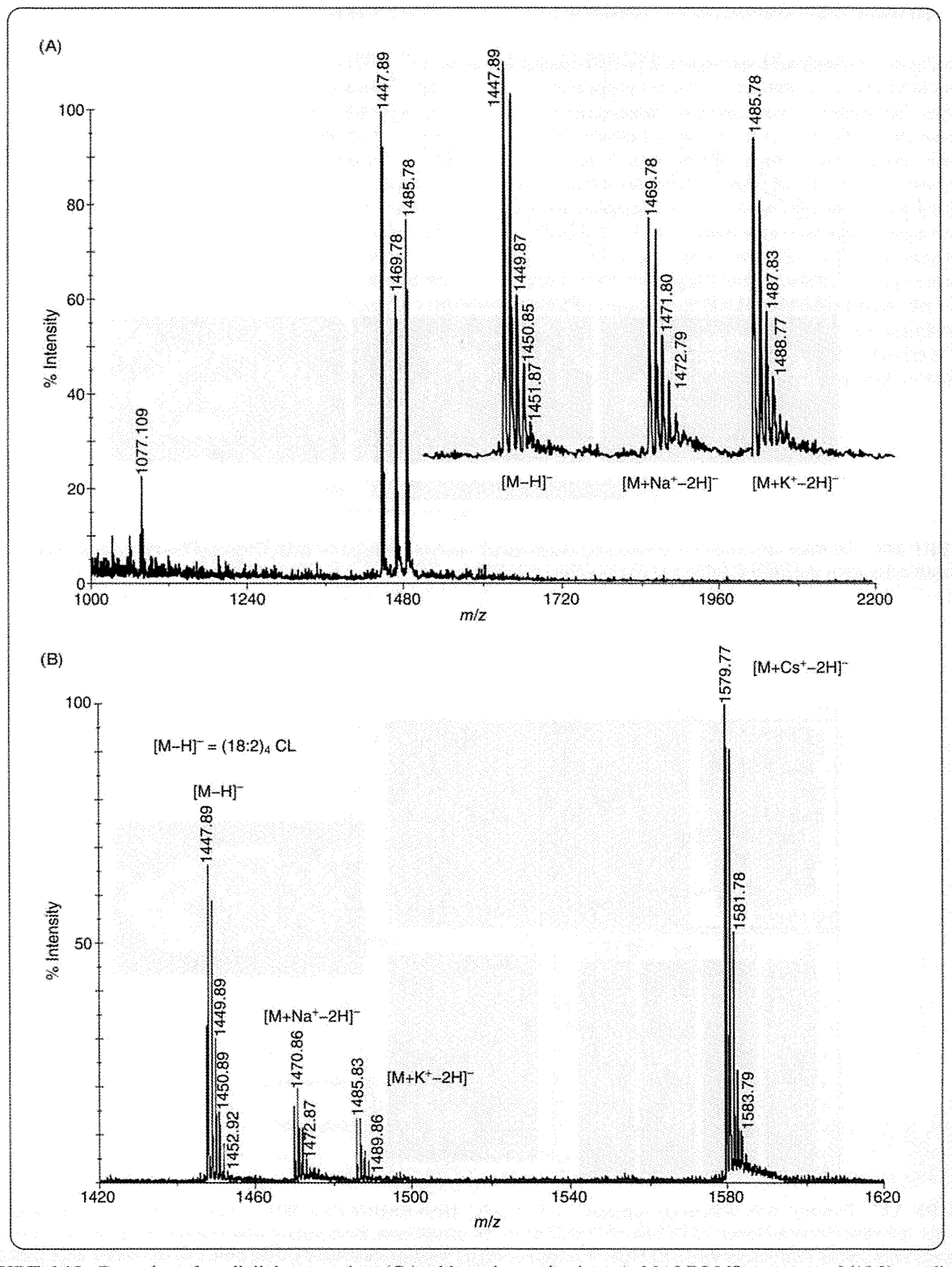

FIGURE 3.15 Detection of cardiolipins as cesium (Cs)-adducted negative ions. A. MALDI-MS spectrum of $(18:2)_4$ cardiolipin (CL) from rat heart section. The inset magnifies the *m/z* region between 1420 and 1520. DHA matrix was used at 30 mg/mL. B. MALDI-MS spectrum of $(18:2)_4$ CL from rat heart section in the presence of Cs ions. The relative abundance of sodiated and potassiated CL was significantly decreased by Cs addition [31].

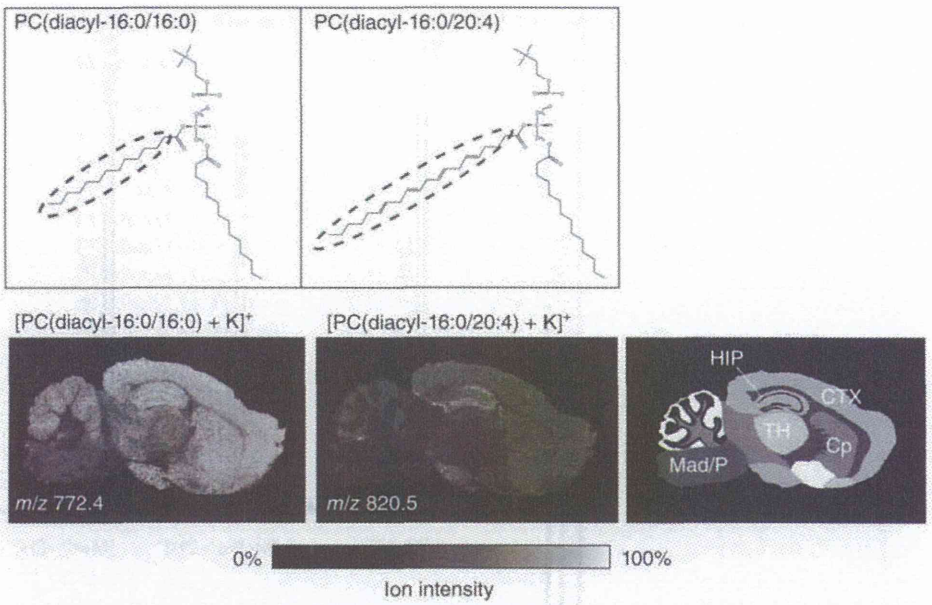

FIGURE 3.16 Distinct localization of phospholipid molecular species revealed by IMS. Different distribution pattern of phospholipids arise from the distinct fatty acid composition of GPLs.

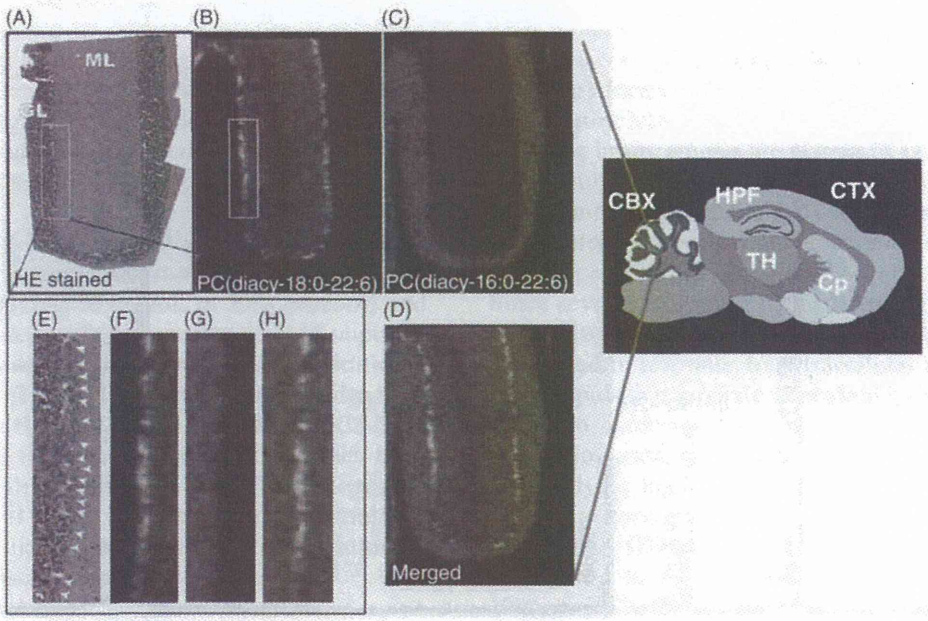

FIGURE 3.17 Purkinje cells selectively contained a DHA-PC. High-magnification IMS at raster size of 15 μm revealed the Purkinje cell-selective distribution of PC(diacyl-18:0/22:6) in the cerebellum. Both optical observation of HE-stained successive brain sections (A, E) and ion images of DHA-PCs (B, F) clearly suggest that the PC was enriched in the Purkinje cell layer (arrowheads). Interestingly, a complementary distribution of another abundant DHA-PC, PC(diacyl-16:0/22:6), was enriched in the granule layer of the cerebellum (C, G). D. Merged image. ML, molecular layer; GL, granule layer; W, white matter; CBX, cerebellar cortex; CP, corpus striatum; CTX, cerebral cortex; HPF, hippocampal formation; TH, thalamus [41].

abundant DHA-PCs, PC(diacyl-16:0/22:6) and PC(diacyl-18:1/22:6), was observed in the granule cells of the cerebellum (Figure 3.17c,d). Such cell-type heterogeneity of the fatty-acid constituent in part reflects the cells' heterogeneous membrane properties. Because of its high degree of unsaturation, DHA-GPLs increase membrane fluidity and even regulate the functions of membrane-associated proteins [42–44]. Purkinje cells are the largest neurons in the brain, with intricately elaborate dendritic arbors. Thus, higher membrane fluidity may be required for effective transport of membrane-associated proteins via the plasma membrane. Thus, the high-level expression of a DHA-PC may contribute to the transportation of membrane proteins in the cells.

3.2.2.3 *IMS of Endogenous Metabolites: Gangliosides*

Gangliosides are glycosphingolipids consisting of mono- to polysialylated oligosaccharide chains of variable lengths attached to a ceramide unit. They are inserted in the outer layer of the plasma membrane, with the hydrophobic ceramide moiety acting as an anchor while their oligosaccharide moiety is exposed to the external medium [45]. Gangliosides also comprise a large family; their constituent oligosaccharides differ in glycosidic linkage position, sugar configuration, and the contents of neutral sugars and sialic acid. Along with the oligosaccharide unit, the ceramide moiety of gangliosides also varies with respect to the type of long-chain base (LCB) (sphingosine base) and the fatty acid to which it is coupled (Figure 3.18).

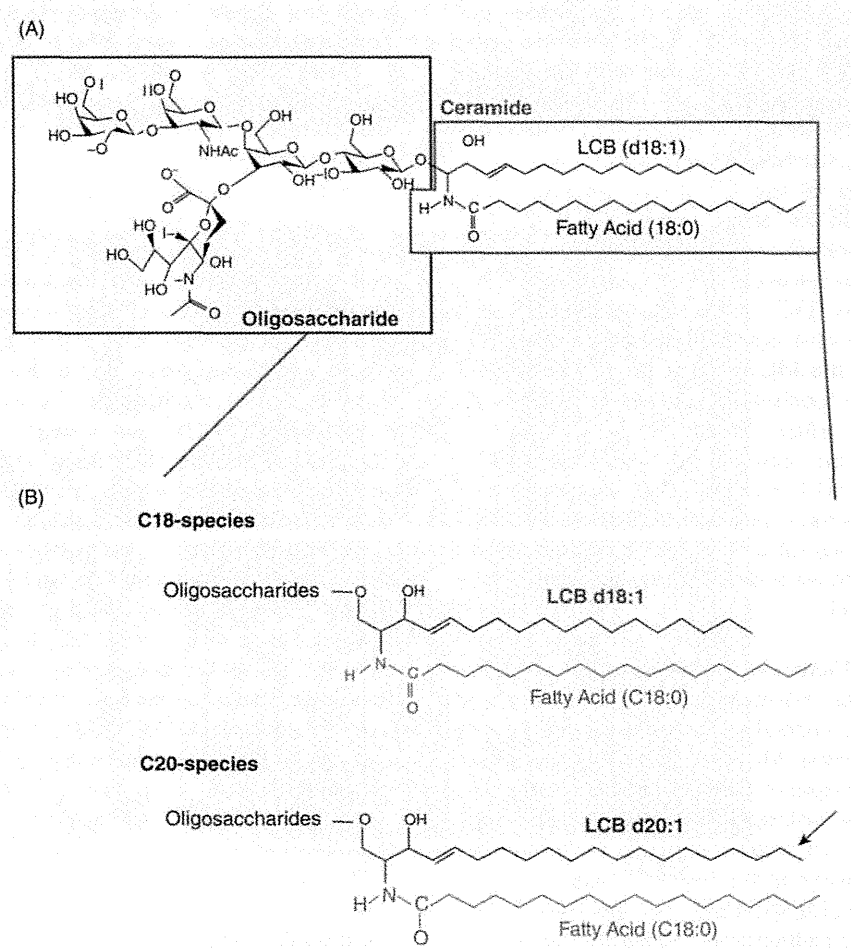

FIGURE 3.18 Structure of GM1a. Gangliosides comprise a large family; their oligosaccharides structures differ in the glycosidic linkage position, sugar configuration, and the contents of neutral sugars and sialic acid content. The ceramide moiety of gangliosides also has some variation with respect to the type of long-chain base (LCB) (sphingosine-base) and fatty acid moiety (A). Structures of ganglioside molecular species containing C18- and C20-long chain base (LCB) are shown in (B).

Previous biochemical studies have revealed that the LCB of the brain ganglioside species has either 18 or 20 carbon atoms (i.e., C18- or C20-sphingosine), and C20-sphingosine (C20-LCB species) is present in significant amounts only in the central nervous system [46–49]. The LCB content increases significantly in rodents and humans throughout life [50–52]. The C20-LCB gangliosides are of great interest because of their characteristic brain specificity and their dramatic increase during the organism's life span. However, the field lacks the capability to provide a precise tissue distribution of C18 and C20 gangliosides. Antibodies to some oligosaccharide moieties are available for visualizing the molecular species with different constituent oligosaccharides [53], but such immunological methods cannot detect the differences in the ceramide structure hidden in the lipid bilayer.

Due to the negative charge on the sialic acids and their rich abundance in the brain, gangliosides are easily detected in the *m/z* 1500–2500 range with IMS in the negative ion detection mode [54–56]. In addition, IMS discriminates not only structural differences in oligosaccharides but also in the lipid moiety, and therefore, the specific distribution of the C20-LCB species is successfully revealed in the mouse brain. While the C18 species is widely distributed throughout the frontal brain, the C20 species is selectively localized in the ML of the dentate gyrus (DG) (Figure 3.19). Furthermore, the developmental- and aging-related accumulation of the C20 species in the ML-DG can be visualized [55], therefore the tissue location of C20 gangliosides accumulation can be identified (Figure 3.20).

These observations indicate that this brain region-specific regulation of LCB chain length is, in particular, important for its distinct function in the brain. As this study clearly demonstrates, the novel capabilities of IMS could shed light on long-standing questions in the biological/clinical field.

3.2.2.4 IMS of Endogenous Metabolites: Primary Metabolites In the body, primary metabolites are directly involved in normal growth, development, and reproduction processes. Most of these molecules are smaller than typical lipids (<*m/z* 600) and regarding the imaging of such low molecular weight compounds, one of the disadvantages of organic matrices is the number of observed mass peaks in the low *m/z* range. The low *m/z* region of a MALDI spectrum contains a large population of ions from endogenous metabolites as well as matrix-related adduct clusters and fragments which are clearly seen in the MALDI ion mobility spectrum obtained on the tissue section [1,57]. Such high density of ions increases the risk for sharing the same mass window by matrix ions and analyte molecules [58] (Figure 3.21). One of the effective solutions to avoid this problem is search and development of the new matrix compounds suitable to the direct-tissue MS.

Recently, 9-aminoacridine (9-AA) was found to exhibit very few matrix interferences in the low-mass range (*m/z* < 500) [59] and thus primary metabolites can be visualized in a MALDI imaging experiment [60,61]. Benabdellah et al. reported that with appropriate sample preparation protocol, 9-AA exhibits almost no matrix interference, and they successfully detected and identified 13 primary metabolites (adenosine monophosphate [AMP], adenosine diphosphate [ADP], adenosine triphosphate[ATP], uridine diphosphate-N-acetylglucosamine [UDP-GlcNAc], etc.) on the rat brain section in the negative ion detection mode [61]. In another report, Burrell et al. also demonstrated that, by use of the 9-AA in positive ion detection mode, localization of sugar and phosphorylated metabolites such as glucose-6-phosphate can be clearly imaged in plant seeds [60].

Here again, we would like to emphasize that the optimization process of the matrix solution is the critical issue; Figure 3.22 demonstrates that only with appropriate solution composition could the adenosine nucleotides be detected significantly. Before imaging experiment, we have to test several solution compositions with consideration of the solubility, pH stability and heat stability of the target analytes, but since the analyte is cocrystallized with numerous other biomolecules on the tissue surface, in practical, the optimal condition is different from that of purified sample of the same molecule. Actually, as shown in Figure 3.22, we found that 70% ethanol solution is the best for the nucleotides though they have low solubility to such organic solvents. In addition, we also observed that trifluoroacetic acid (TFA) in the solution severely prohibited the ionization of the nucleotides. We eventually determined the optimized condition as 9-AA (10 mg/mL) in the 70% ethanol. Adenosine nucleotides, especially ATP, is well known as the "molecular unit of currency" of intracellular energy transfer [62]. Cellular metabolic processes that use ATP as an energy source convert it into ADP and AMP; therefore, simultaneous imaging of these molecules by IMS provides valuable information regarding tissue metabolic activity. As shown in Figure 3.23, we could simultaneously visualize the distribution pattern of ions for AMP, ADP, and ATP, and furthermore, MS/MS analysis successfully validates these molecular assignments. Finally, we additionally note that because of the in-source decay, the phosphate groups of ATP and ADP may be dissociated and they could be detected as ADP and AMP. In this context, further studies to suppress the in-source fragmentation of phosphate groups are the next issue to consider.

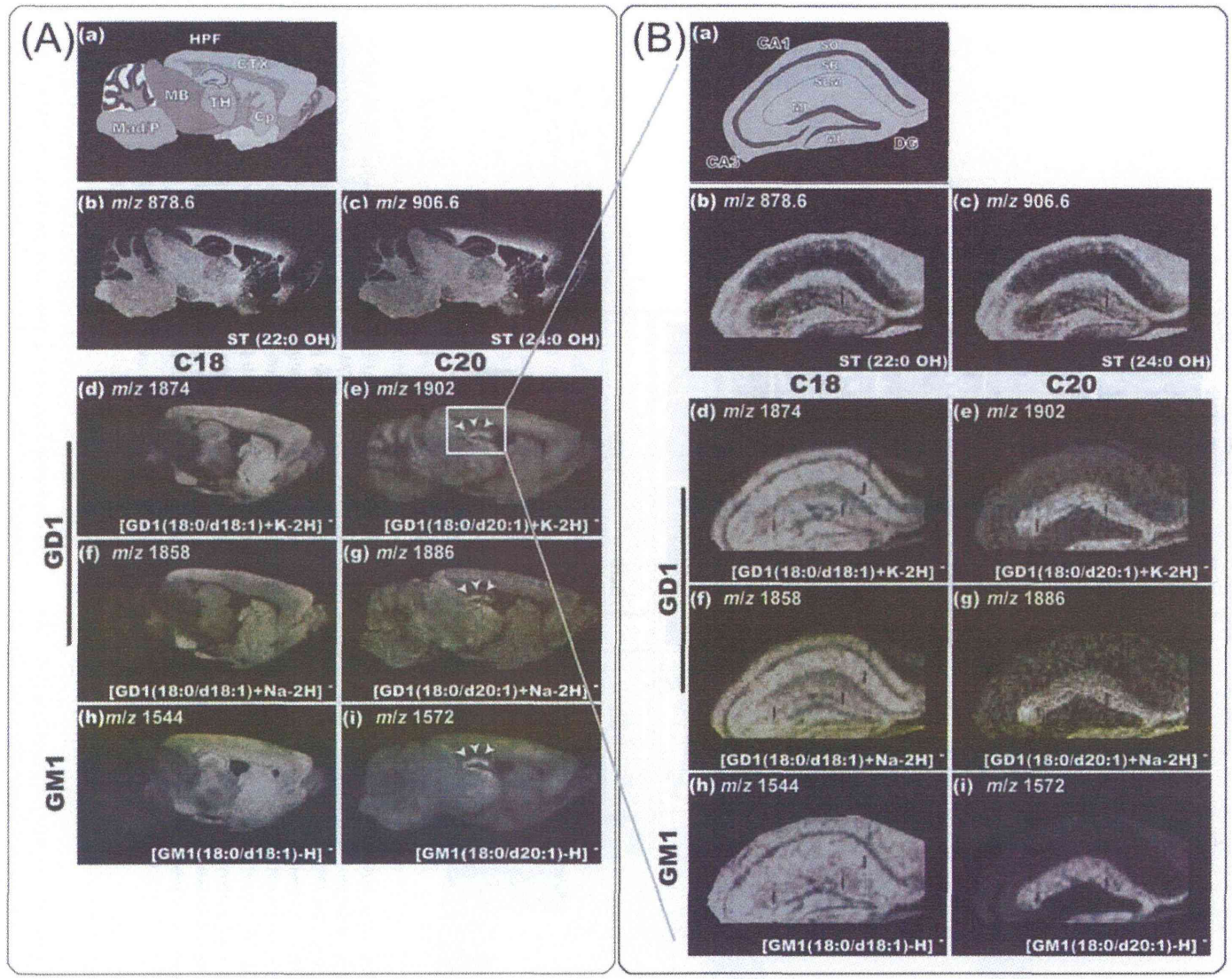

FIGURE 3.19 Localization of C20-sphingosine-containing gangliosides in the hippocampal formation. A. IMS at 50 μm raster step size was used to gain an overview of ganglioside distribution in different brain regions. B. IMS at 15 μm raster size was used to study in detail the distribution pattern of gangliosides in the hippocampus. In both panels, the schematic diagram of the brain section (a) and ion images of STs (b and c) are presented. For ions corresponding to the GD1 molecular species, the ion distributions of both sodium and potassium complexes, that is, the ions at *m/z* 1858 (f) and *m/z* 1886 (g), which correspond to the $[M+Na-H]^-$ form of C18- and C20-GD1, and those at *m/z* 1874 (h) and *m/z* 1902 (i), which correspond to the $[M+K-H]^-$ form of C18- and C20-GD1, respectively, were observed. The ion distribution patterns corresponding to the GD1-Na salts and GD1-K salts are fairly uniform for both C18- and C20-species. For GM1, *m/z* 1544 (d) and *m/z* 1572 (e), which correspond to C18- and C20-sphingosines containing GM1, respectively, are shown.

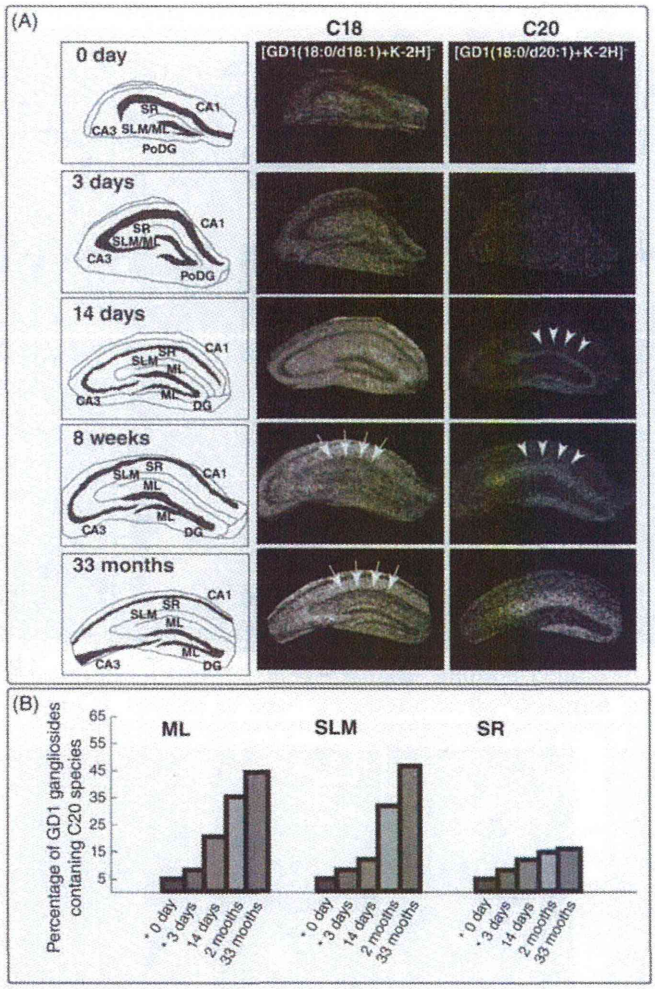

FIGURE 3.20 Development- and aging-related accumulation of C20-GD1 in the ML and stratum lacunosum moleculare (SLM) of the hippocampal formation. It was visualized that the ion corresponded to GD1 (*m/z* 1874 and 1902) in the mouse hippocampus at the indicated time points (P0, P3, P14, 1 month, and 33 months). For each time point, the intensity scale of C20-GD1 is normalized in order that the brightest pixels of C20-GD1 have 60% of the maximal C18-GD1 intensity value. In the P14 mouse hippocampus, C20-GD1 was concentrated in the narrow area of dentate gyrus–middle layer of stratum moleculare (DG-SMm) and began to spread over the medial edge of the region (arrowheads). In contrast, the concentration of the C-18 species decreased in the ML/SLM with aging (arrows). Quantification result of C20-GD1 on the total GD1 signal in the ML, SLM, and stratum radiatum (SR) regions has also been shown (B). *At P0 and P3, we could not distinguish between the ML and SLM areas; therefore, values obtained from the region corresponding to ML/SLM have been used for both regions in the graph.

3.2.3 IMS of Exogenous Drugs

In drug discovery and development, it is a crucial process to determine how a candidate compound is distributed and metabolized within the body. The use of IMS to monitor drug delivery and their metabolism has also been attractive application area. IMS offers detailed drug distribution images, which are comparable to traditional whole body autoradiography (WBA) technique using radiolabeled compounds (Figure 3.24). Stoeckli et al. show these two methods produce remarkably similar results, by performing the IMS and WBA using whole-body sections of the same rat after intratracheal administration of a compound (0.5 mg/kg); intense signals are detected in the trachea, the lung, and the stomach while low levels are detected in the blood, and this reports have nicely introduced the usefulness of IMS for pharmacology.

In addition to that, IMS provides several advantages for determining drug distribution. First, MS-based

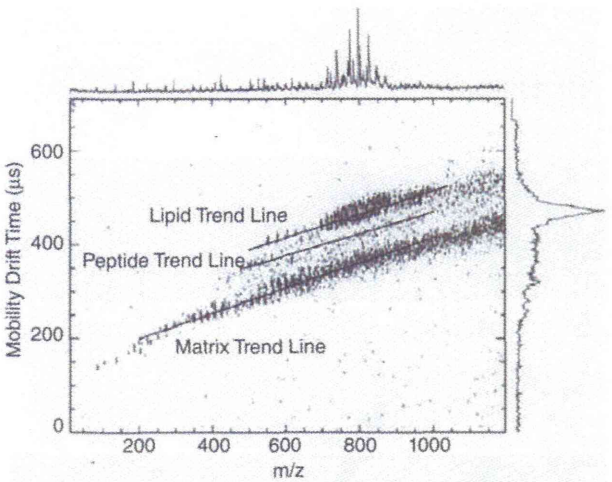

FIGURE 3.21 MALDI-ion mobility 2D plot of a rat brain tissue section with DHB matrix in positive ion detection mode. Many of the peaks in the trend line identified as "matrix" can be assigned to DHB clusters or DHB clusters + potassium. Reprinted from Jackson et al. [58].

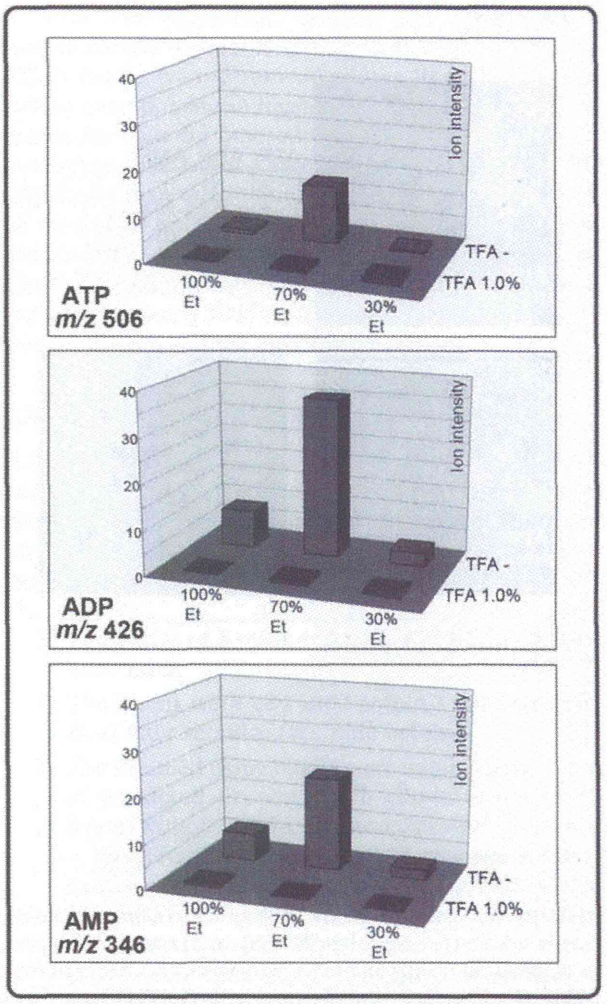

FIGURE 3.22 Optimization of solvent composition for IMS of nucleotides. On the tissue section of mouse heart, AMP, ADP, and ATP were profiled by MALDI-IMS with 9-AA (10 mg/mL) dissolved into different solvent composition of matrix solution. One microliter (1 μL) of each matrix solution were spotted on the sections, and these matrix spots were raster scanned. Indicated ion intensities for AMP (at *m/z* 346), ADP (at *m/z* 426), and ATP (at *m/z* 506) were obtained from averaged mass spectra of each spots. Et, ethanol.

molecular detection enables simultaneous and discriminative monitoring of both the intact drug molecules and their metabolites [2,57]. By its nature, WBA cannot distinguish these molecules. In this regard, IMS can determine whether medicinally intact drugs have reached the target organs. Moreover, IMS can provide a visual distribution of drugs at a lower cost and in a much shorter time than detection using isotopes [63]. Khatib-Shahidi et al. have successfully investigated the distribution of olanzapine and its metabolites in a whole rat sagittal section 2 and 6 h after administering the dose [2]. This study clearly showed the distinct distribution of intact drugs and their metabolites; the intact drug reached the target organ (the brain), whereas its metabolites were localized in the bladder. Furthermore, the time course of the metabolism of parent drugs into demethylated and hydroxymethylated metabolites were visualized over the whole-body section. In this study, notable decreases of olanzapine were observed everywhere in the body except the testis and bladder, while the metabolized compounds accumulated in the bladder [2] (Figure 3.25). This example demonstrates that IMS-based drug monitoring provides valuable information for drug development.

On the other hand, ion suppression effects should be considered. In fact, Stoeckli and colleagues have shown that there are small regions (although less than 5% of the total region) where the drugs could not be detected, presumably because of ion suppression effects using a mouse whole-body section coated with analyte drugs [63]. Thus, optimization of the sample condition so that the analyte molecule present in the crude mixture can be efficiently ionized is an important issue. For this purpose, sample preparation has a critical role. In particular, it is helpful to perform a preliminary experiment using a reference drug because the choice of a suitable matrix compound, as well as optimizing the composition of the matrix solution, can improve the ionization efficiency of the molecules of interest.

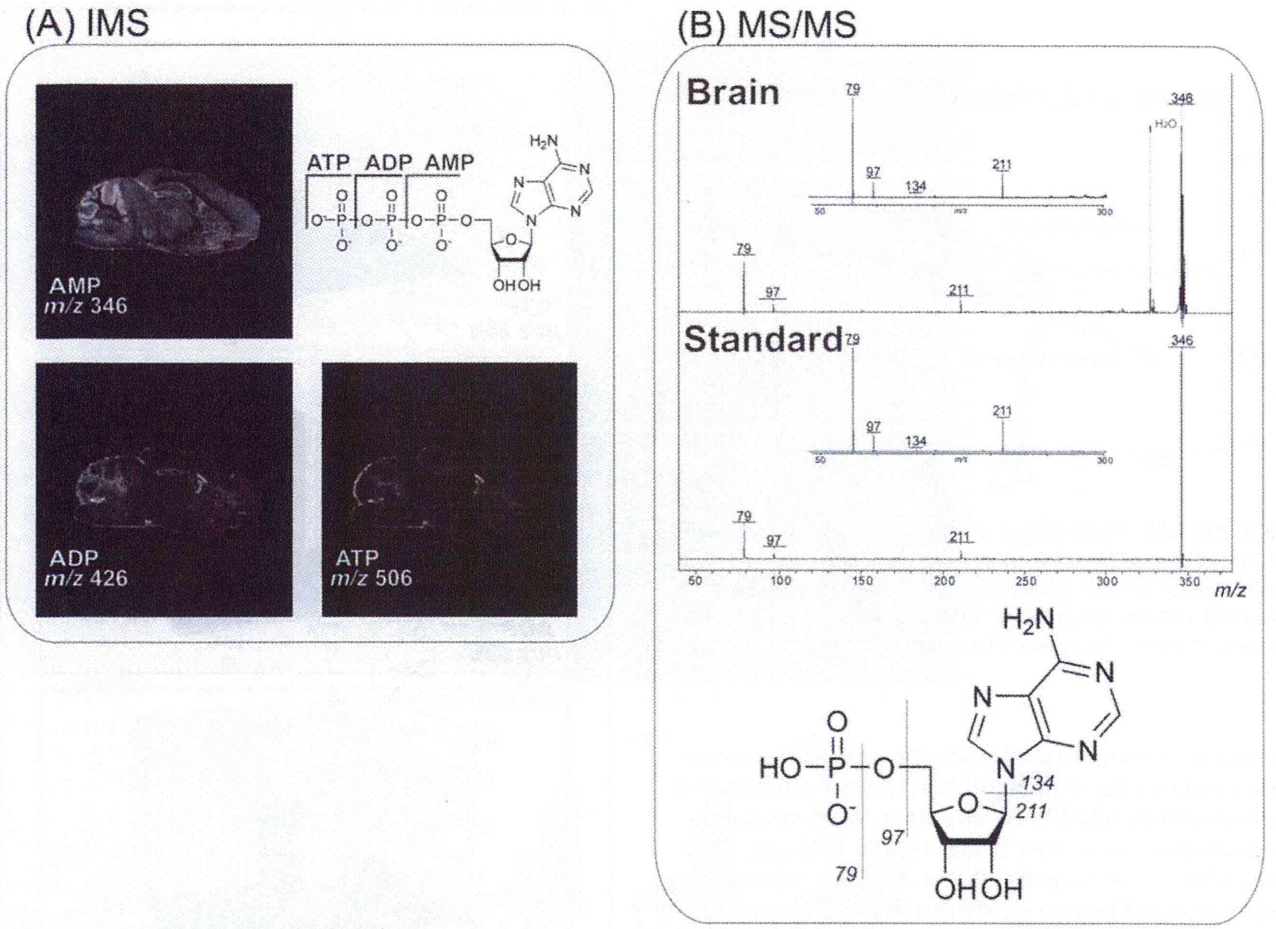

FIGURE 3.23 MALDI-IMS application to adenosine nucleotides. A. Imaging results for AMP, ADP, and ATP with use of 9-AA matrix solution (10 mg/mL in 70% ethanol) at raster scan pitch of 80 μm. B. MS/MS results of the precursor ion at *m/z* 426 acquired from standard sample and brain tissue section. Observed fragmentation pattern indicates that the precursor ion was derived from $[AMP\text{-}H]^-$. The data were obtained with TOF/TOF instrument (Ulatra FlexIII, TOF/TOF, Bruker Daltonics).

3.3 EXPERIMENTAL PROCEDURES

In this section, we will introduce the principle and overview of MALDI-IMS and its representative applications. In the following part, the detailed IMS experimental procedures and practical point-to-point techniques will be described; especially for the major IMS application that involves protocol for PC and gangliosides, their results are shown in Figures 3.16, 3.17, 3.19 and 3.20, respectively.

3.3.1 Materials

3.3.1.1 Chemicals

1. TFA
2. 1,2-dihexanoyl-*sn*-glycero-3-phosphocholine (MW: 453.5, monomer and dimmer were used for calibration) and peptide calibration standard II (Bruker Daltonics, Leipzig, Germany; covered mass range: ~700–3200 Da) as a calibration standard
3. DHB (Bruker Daltonics) as a matrix

Note: All of the chemicals used in this study were of the highest purity available.

3.3.1.2 Matrix Solution for MALDI-IMS of PCs For measurement of PC, a DHB solution (40 mg/mL DHB, 10 mM potassium acetate, 70% methanol, 0.1% TFA) was used as the matrix solution [41].

3.3.1.3 Matrix Solution for MALDI-IMS of Gangliosides For measurement of gangliosides, a matrix solution without salt (40 mg/mL DHB, 70% methanol, 0.1% TFA) was used as the matrix solution [55].

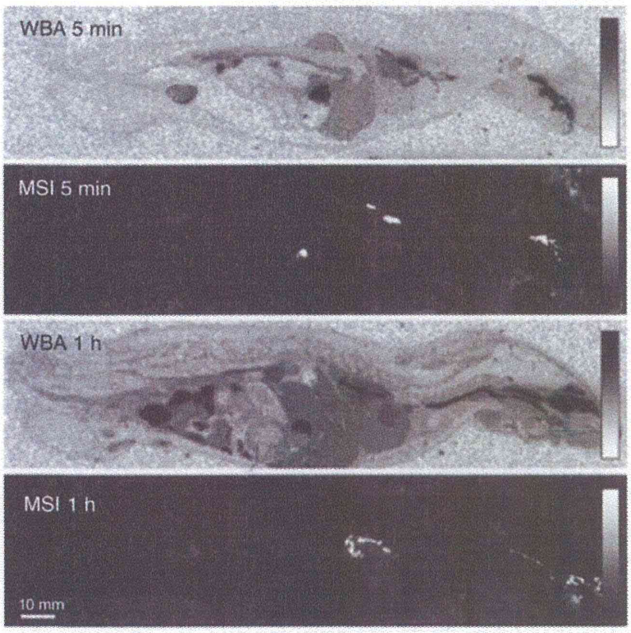

FIGURE 3.24 Comparison of IMS with WBA using whole-body sections after intratracheal administration of a compound (0.5 mg/kg) to rats. The two corresponding sections are from the same animal, but from different positions. Comparison of the methods shows remarkable similarity in the results: high levels are detected in the trachea, the lung, and the stomach, and lower levels in blood. MSI (mass spectrometry imaging) is used as a synonym of IMS [63].

Note: The potassium, sodium, and lithium alkali metals show a distinct ability to form adducts with the PC molecule. We recommend adding 10 mM potassium salt because potassium forms a stronger adduct with PC molecules than did other metals. Figure 3.26 shows that potassium ions formed stronger adducts with the PC molecules than did sodium and lithium ions. Addition of 10 mM of potassium acetate to the matrix solution resulted in the dominant formation of the $[M+K]^+$ ion. On the contrary, other types of PC ions still accounted for approximately 50% on total intensity after the addition of 20 mM sodium and lithium acetate.

3.3.2 Methods

3.3.2.1 Animal Sacrifice and Tissue Extraction All experiments involving mice were conducted in accordance with the protocols approved by the animal care and use committee at the participating research institute.

1. The brains of 8-week-old male C57BL/6J Cr mice were used.
2. The brains were extracted within 1 min (typically 40 s) after sacrifice (see note below).
3. The trimmed tissue blocks were immediately frozen in powdered dry ice, which allows tissues to be frozen without cracks, and stored at –80°C until use.

   Note: As shown in Figure 3.27, postmortem degradation of GPLs was observed by IMS within 15 min in a series of mouse brains extracted at different times (15, 30, 60, and 120 min). This is presumably because of stimulation of phospholipase enzymes under ischemic conditions [64,65].

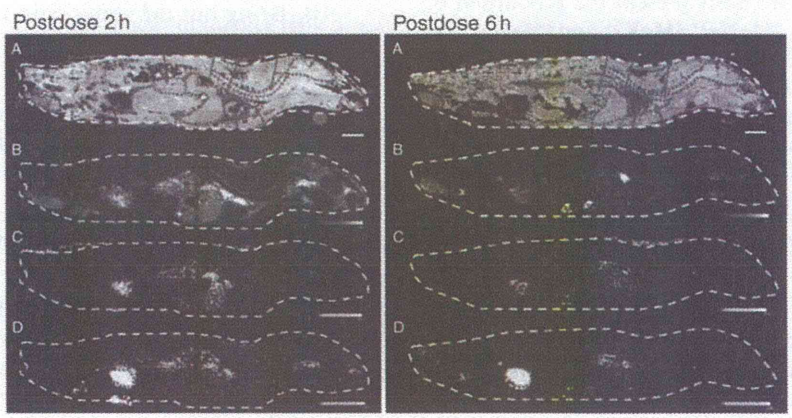

FIGURE 3.25 Detection of the drug olanzapine and its metabolite distribution in a whole-body sagittal tissue section by single IMS analysis [2]. A. Optical images of tissue sections from rats 2 and 6 h after treatment with olanzapine, across four gold MALDI target plates. Organs are outlined by dashed lines, and a dot is used as a time point label. B. MS/MS ion image of olanzapine (*m/z* 256). C. MS/MS ion image of N-desmethyl metabolite (*m/z* 256). D. MS/MS ion image of 2-hydroxymethyl metabolite (*m/z* 272). Bar denotes 1 cm.

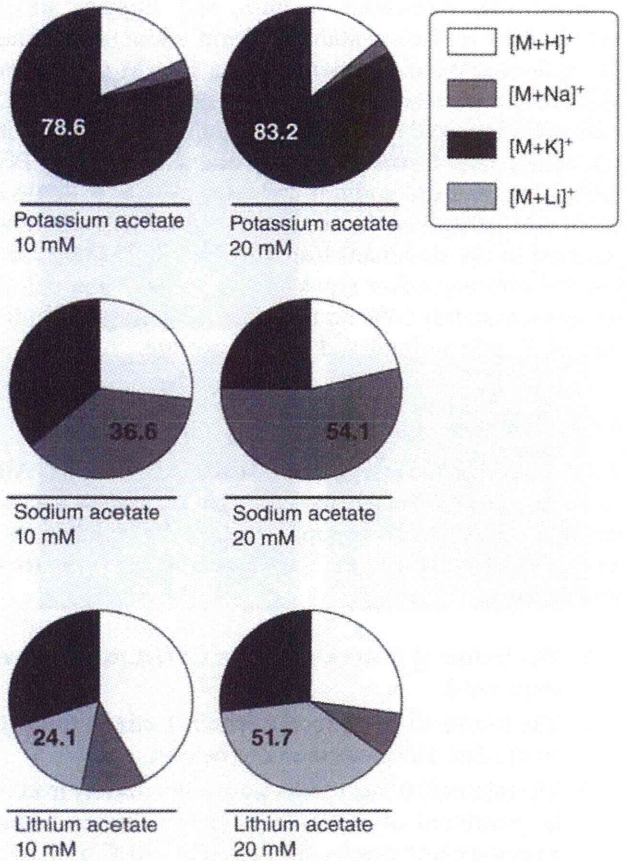

FIGURE 3.26 Potassium forms a stronger adduct with PC molecules than did sodium and lithium. To determine optimum experimental condition of using alkali metal salt as matrix additive, we added potassium, sodium, and lithium salts in various concentrations to the matrix solution. We then sprayed matrix solutions containing potassium, sodium, and lithium acetate in various concentrations (10 and 20 mM) on the tissue sections. The circular charts present the proportion of ion intensities of $[M+H]^+$, $[M+Na]^+$, $[M+K]^+$, and $[M+Na]^+$ ion of lyso-PC(17:0), which was dispensed on the brain homogenate slice ($n = 3$). Potassium dominantly formed an adduct with the PC molecule upon addition of 10 mM potassium acetate; on the other hand, other types of PC ions still accounted for approximately half upon the addition of 20 mM sodium and lithium acetate.

3.3.2.2 Preparation of Tissue Sections The process of preparing sections for IMS measurement is essentially similar to that used in the preparation of frozen sections for immunostaining or dye staining. However, since the sections created in this case are served to MS measurement, there are certain essential differences compared to the section-preparation techniques used in other staining methods, as summarized in Table 3.5. A point to bear in mind is that IMS is an imaging technique based on MS, a microchemical analytical technique.

1. Usually, tissue blocks are held by an optimum cutting temperature (OCT) polymer, but tissues should not be embedded into such polymer reagent because any residual polymer on the tissue slices degrade the mass spectra for both protein and small molecular analysis [10] (see Note 1).
2. Wipe off any oil remaining on the blade with ethanol and carefully attach the blade to the cryostat (here we used CM 3050; Leica, Wetzler, Germany).
3. Precool the forceps and brushes by placing them inside the cryostat.
4. Adjust the several conditions of cryostat and try sectioning. (e.g., the position of the antiroll and blade, angle of the sample, and chamber temperature, etc). If sections tend to curl up, the temperature is too high or the antiroll is placed inappropriately (Figure 3.28).
5. In this study, tissues blocks were sectioned at –16°C to a thickness of 5 μm [10,66].
6. Try cutting and determine the optimal tissue thickness (see Note 2).
7. Keep the slice under the antiroll for a while, until it no longer curls.
8. Put the ITO-coated glass slides (Bruker Daltonics) into the chamber, immediately place the slides over the tissue slice, and paste tissues on it (Figure 3.28).
9. Keep performing thin-sectioning and pasting.
10. Bring out the slides with tissues, and immediately dry them in a stream of nitrogen gas. Insufficient drying causes the sample to peel off.
11. Serve the slice to the next process (washing process for protein analysis or matrix application for small molecule analysis).

Notes:

1. Embedding enables the sample to retain its shape and makes the cutting process easier. However, in IMS experiments, attachment and penetration of the embedding agents (e.g., OCTs) in the samples can lead to a deterioration of the MS signals [4,10] (Figure 3.29A). In particular, when analyzing small molecules with an m/z 800–2000, contamination with OCT highly abundant signals that correspond to the polymer in the positive ion